FLIGHT LOADS ANALYSIS AND MEASUREMENTS OF EXTERNAL STORES ON AN ATMOSPHERIC RESEARCH AIRCRAFT

Vega Handojo[1], Thomas Klimmek[1], and Wolf Krüger[1]

[1] DLR - German Aerospace Center
Institute of Aeroelasticity
Bunsenstr. 10, 37073 Göttingen, Germany
Vega.Handojo@dlr.de

Keywords: flight loads, aeroelasticity, turbulence.

Abstract: The research aircraft DLR HALO (High Altitude and Long Range Research Aircraft) is able to carry external stores. These stores are mounted at the wing hardpoints and can house several measurement instruments for atmospheric research. However, to ensure the safety and structural integrity of the aircraft and the stores, modifications on the aircraft have to be investigated with numerical analyses and experimental data. The DLR project iLOADS aims at the development of an internal DLR loads process, among others also to be able to support certification capabilities for the DLR aircraft fleet. To assist the DLR HALO operations, a simulation model of the aircraft was set up and loads analyses have been carried out in the Institute of Aeroelasticity at DLR Göttingen. For the experimental part, a flight test campaign with DLR HALO has been performed in April 2016, totaling 14 flying hours. In the test flights strain data of wing external stores, acceleration data of installed sensors and turbulence data were collected. First analyses have been carried out and the findings can be utilized in the further development of the DLR loads process.

NOMENCLATURE

F	: force in general
M	: moment in general
n	: number of loads applied
P	: loads in general
q	: number of strain gauge bridges taken into account
wg	: vertical wind speed
β	: load coefficient
γ	: probable error
ε	: residual between calculated and applied load
μ	: strain signal

1 INTRODUCTION

The determination of loads acting on the aircraft is one of the main tasks during aircraft development. The knowledge of loads is important for aircraft design; not only for certification, but also because the structural weight is influenced by the loads themselves. For that reason the definitions of realistic loads assumptions as well as the generation of loads from simulation and experiment are of importance. DLR has strong activities in aircraft

preliminary design and in the operation of a fleet of research aircraft, and thus requires expertise for the definition and the determination of sizing relevant load cases.
The DLR project iLOADS aims at the development of an internal DLR loads loop, comprising expertise from different DLR institutes. The goal of the process is to improve the assessment capabilities of DLR with respect to the influence of loads on new aircraft configurations, and to support certification capabilities for the DLR aircraft fleet. For the DLR aircraft HALO, which is a modified Gulfstream G550 and mainly used for atmospheric research within the German research community, loads flight testing has been done in order to further develop the DLR loads process.
The HALO is an aircraft fully certified by Gulfstream Aerospace Corporation (GAC), and the certification has been extended by DLR and partners to fly with a so-called belly pod. The belly pod is used for equipment under the fuselage, and provisions on the fuselage for a number of external sensors such as cameras or trace gas collectors. For additional equipment, so-called PMS-carriers (Particle Measurement System), special wing stores designed for atmospheric research, can be attached under the wing at specially prepared stations.

Figure 1. HALO research aircraft during flight test campaign

The flight test campaign has been performed in April 2016. The main objectives were the validation of the approach and methods used for the HALO loads analysis and the further development of the online monitoring capabilities of DLR-AE (DLR Institute of Aeroelasticity) regarding aircraft modal parameters during flight, described by Sinske et al. [1] and Schwochow et al. [2]. During the campaign five test flights were performed, with a flight duration of 90-180 minutes each and a total flight duration of around 14 hours. In the first, third, fourth and fifth flight mainly in-flight analysis to determine structural dynamic characteristics was performed [1].
The second flight was designated for flight loads measurement, which is the main topic of this work. The loads flight testing is intended to improve and validate the DLR simulation models und methods for realistic loads analyses complying also with the requirements given by the regulations (e.g. CS25) [3]. Hereby primarily the measurement and simulation of interface loads between the wing and the PMS carrier is of concern. The loads were induced among others by flying roll and pull-up maneuvers, in total at seven different altitudes and with three airspeeds each.

2 AIRCRAFT LOADS SIMULATION MODELS AND ANALYSIS

For the loads analysis of the aircraft, DLR simulation models were set up with the DLR MONA process. MONA [4],[5] is a combined loads and design process, stands for ModGen and MSC Nastran, which are the two main programs used in the process. Therein loads are estimated and subsequently used for various dimensioning methods such as structural optimization of each aircraft component.
ModGen is an in-house program at DLR-AE, which is used to set up simulation and optimization models for the loads analyses and the structural optimization. The latter can be applied on particular aircraft components or the complete aircraft configuration. The model set-up is based on a parametric approach to enable an accurate generation of structural models while providing a wide range of variation possibilities. All simulation and the structural optimization task of the MONA process are carried out with MSC Nastran.
To set up the structural model for the DLR HALO a modified MONA process was established as presented in Figure 2. In the first step the geometry and the structural design of each component were parameterized with ModGen. Hereby data from GAC and DLR such as geometry and structural concept were considered. For the lifting surfaces the structural dimensions were estimated by a preliminary cross section sizing (PCS) method. This is an empirical-analytical method and uses the available cutting loads from GAC. The bending moment *Mx*, the torque *My* and the vertical force *Fz* were transformed into the load reference axis coordinate system and used for the sizing. The sizing parameters comprise the thickness of the skin, the spars, the ribs as well as the dimensions of the stringer and the spar caps. Inner stiffener elements of the spars and ribs were sized according to van Dalen et al. [6]. The fuselage is represented by beam elements and was sized with the method described by Ardema et al. [7]. Therein the diameter of the fuselage sections as well as their stiffener elements were taken into account. The mass model for the minimum empty weight configuration was taken from GAC, while the payload and fuel masses were set up by DLR-AE. The payload mass distribution was carried out according to the rules given by GAC in a mass report. The fuel mass modeling was done with ModGen. For each fuel tank the individual filling levels and deck angles of the aircraft can be considered. The aerodynamics is modeled with the Doublet-Lattice-Method (DLM). The simulation models of DLR HALO are presented in Figure 3.

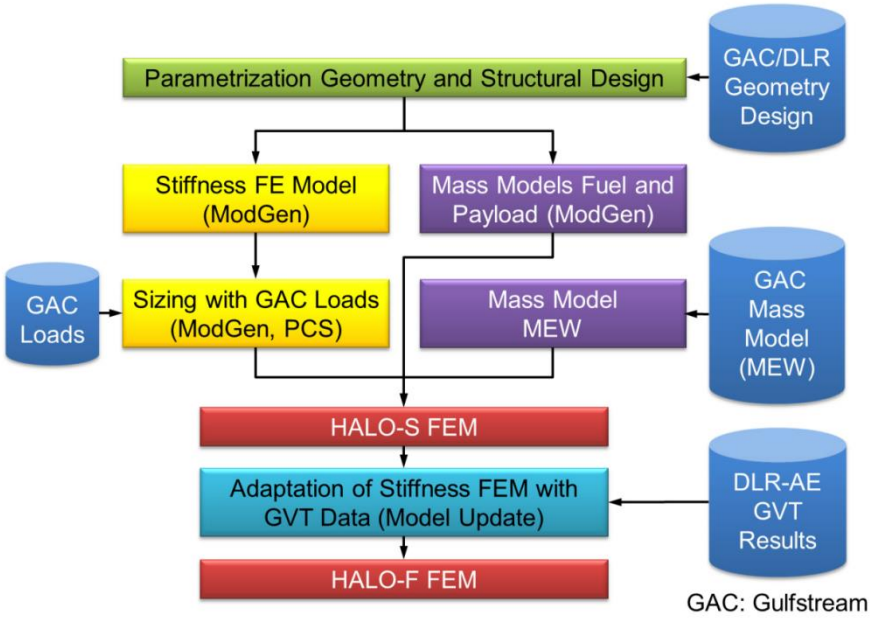

Figure 2. DLR-AE MONA process adapted to DLR HALO

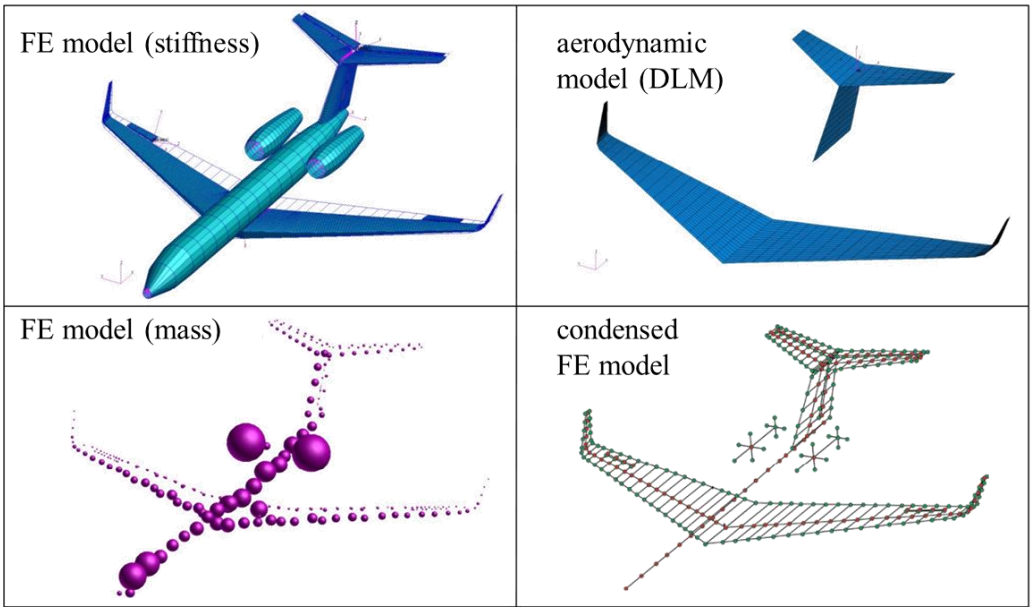

Figure 3. Finite element model HALO-S and aerodynamic model for DLM

Loads simulations based on the certification requirements were performed first for the aircraft without stores. The resulting maximum wing bending moment *Mx* is in average 3% smaller than the data provided by GAC, whereas the largest difference is about 8%. It is assumed that the deviation is mainly caused by the aerodynamic model since a correction of the DLM model was not taken into account yet. Having collected confidence in the model, a finite element representation of the external stores was developed and connected to the aircraft.

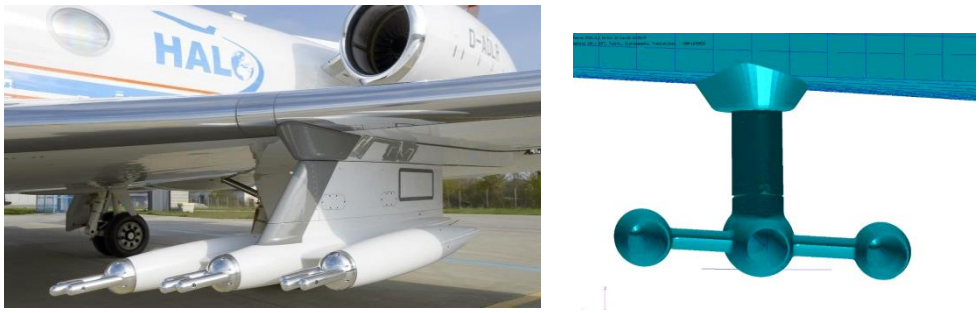

Figure 4. HALO PMS carrier and its simulation model

Gust simulations were performed, with input from standard gust definitions, e.g. classical 1-cos-gusts. As the permitted range for sensor weight and center of gravity in the PMS is defined by the resulting dynamic loads envelope of the carrier, the interface loads between PMS carrier and wing are of special importance as critical quantities.

3 INSTRUMENTATION FOR IN-FLIGHT MEASUREMENTS

For flight testing, the aircraft including the PMS carriers were equipped with accelerometers, as well as with strain gauges at the interface between PMS carrier and wing, the so-called hardpoints. During testing, those quantities could be monitored constantly. In this work the focus lies on the strain gauge measurement.

3.1 Strain gauges

The in-flight loads measurement was performed with the use of strain gauges. On each interface between the external store and the wing, the so-called “hanger beam”, eight strain gauge bridges were placed, which consist of four strain sensors each. Six bridges were wired to detect bending and two to detect torsional deformation. The positions of the bridges were determined with the help of an FE analysis of the hanger beam to acquire measurable deformations under loading. Furthermore, two sensors of one bridge are placed on one side and the other two sensors on the opposite side of the hanger beam, as depicted in Figure 5. The local coordinate system for the hanger beam used in further calculations is shown in Figure 6.

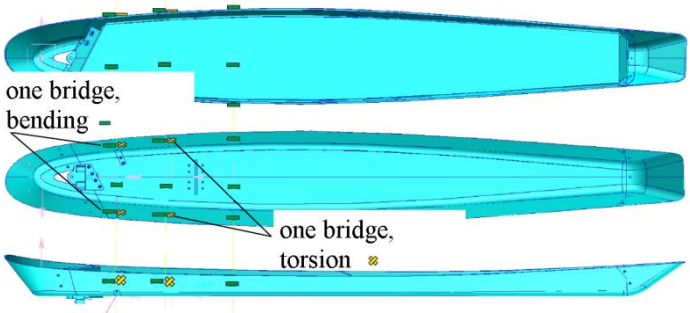

Figure 5. Positions of the strain gauges on the hanger beam

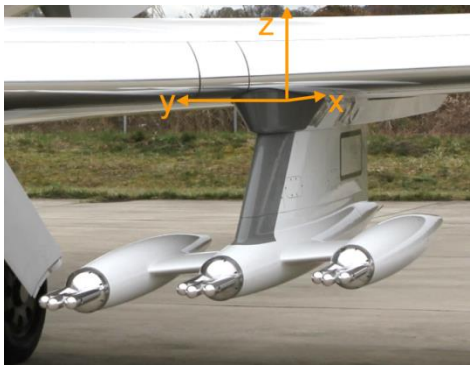

Figure 6. Definition of the local coordinate system on the hanger beam

3.2 In-flight data acquisition

The data acquisition was performed using a combination of three distributed measurement chassis, connected by Ethernet cables, with one board inside the middle tube of each PMS carrier and one in the fuselage. Beside the acceleration and the strain signals, data from the aircraft measuring system BAHAMAS such as airspeed, altitude and angle of attack were also collected. The data were channeled to the data acquisition PC (DAQ-PC) and recorded. From DAQ-PC the data were directed into a network which analysis PCs have access to. A simplified block diagram of the data flow is depicted in Figure 7. A more detailed description of the data acquisition system is presented by Sinske et al. [1].

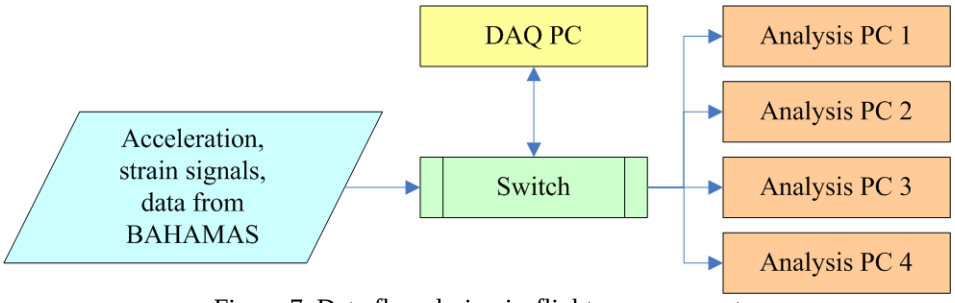

Figure 7. Data flow during in-flight measurement

4 PRELIMINARY TESTS

4.1 Gust simulation on the vibration table MAVIS

One preliminary test for the flight experiment was a hardware gust simulation of the PMS carrier at DLR in Göttingen. For this purpose the PMS carrier was mounted upside down on the vibration table MAVIS (Mehrachsen-Vibrationssimulator, multi axis vibration simulator). The setup is illustrated in Figure 8. The gust load case selected for the simulation is a design load case for the PMS carrier, with a gust gradient of 50 feet (16 m). In order to generate the input signal for the MAVIS, a numerical gust simulation was performed beforehand. In the numerical simulation the PMS carrier was represented by rigid bodies and the hanger beam by an elastic beam. The results in form of deflection, velocities and accelerations were extracted, scaled down and taken as inputs for the gust simulation on the MAVIS. The normalized time responses of the hardpoint displacement and velocity resulting from the numerical simulation are depicted in Figure 9.

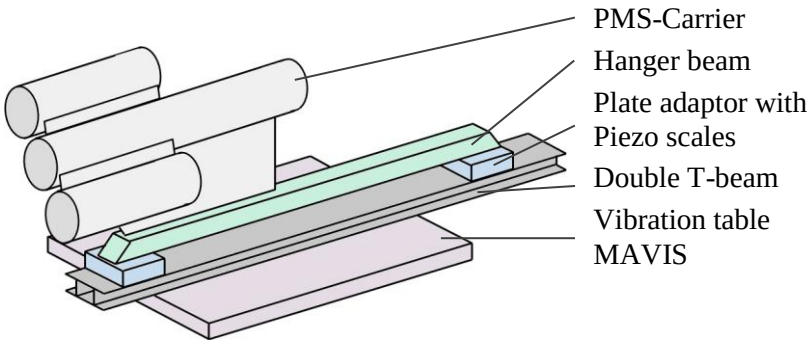

Figure 8. PMS carrier setup on vibration table MAVIS

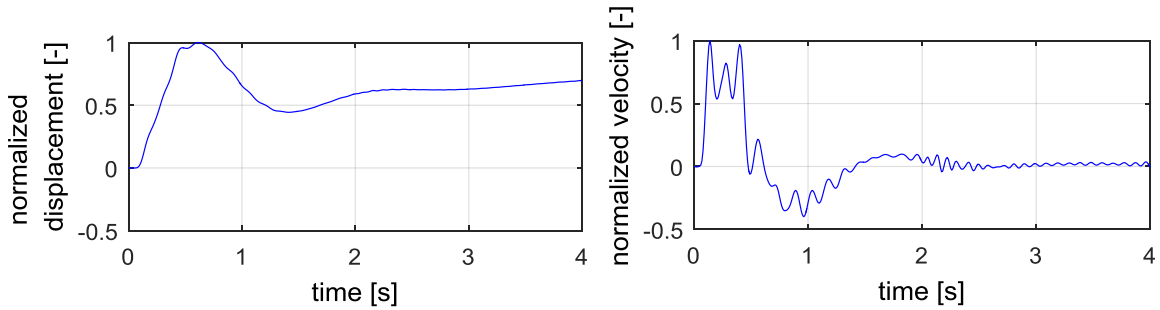

Figure 9. Normalized time responses of the hardpont from a numerical gust simulation

4.2 Strain gauge calibration

With the strain gauges installed, the relationship between the strain signals and the loads acting on the PMS-carrier, which is expressed by the matrix $[\beta]$ in equation (1), is to be identified.

$$P = \mu\,[\beta] \tag{1}$$

With

P:	load vector acting on the PMS-carrier
$[\beta]$:	transfer matrix
μ:	strain signal vector

For that aim a calibration of the strain gauges was conducted by applying non-collinear loads on the PMS carrier and measuring the strain signals. With sufficient numbers of applied loads – more than the number of bridges – the relationship between load and strain signal can be derived [8], which is explained in subsection 4.3.
The first calibration of the strain gauges was carried out at DLR in Göttingen. The load application was conducted with the help of sandbags. Weights of up to 50 kg were attached to each force transmission point. To minimize error due to hysteresis, the applied loads were increased and decreased step by step. The strain signals were measured for each step. A typical strain response of a two-step load case is shown in Figure 10. To ensure that there is no singularity problem in the derivation of the matrix $[\beta]$, each of the six load components – three forces and three moments – has to be included in at least one load configuration.

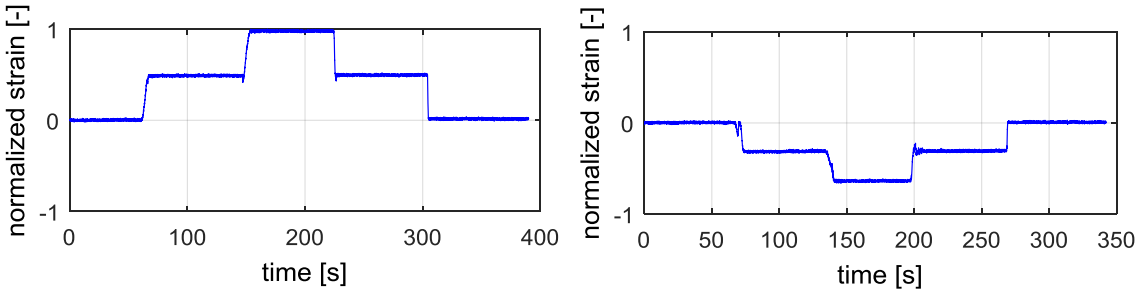

Figure 10. Strain responses of a bridge in two different load cases

The second calibration of the strain gauges was performed at DLR in Oberpfaffenhofen where both PMS carriers were mounted on the wing station of the DLR HALO. In total nine linearly independent loads were applied to each PMS carrier. The load application during the calibration is presented in Figure 11. In addition, an electromagnetic compatibility test and a taxi vibration test were carried out beforehand to ensure the functionality and the safety of the measurement systems in flight [1].

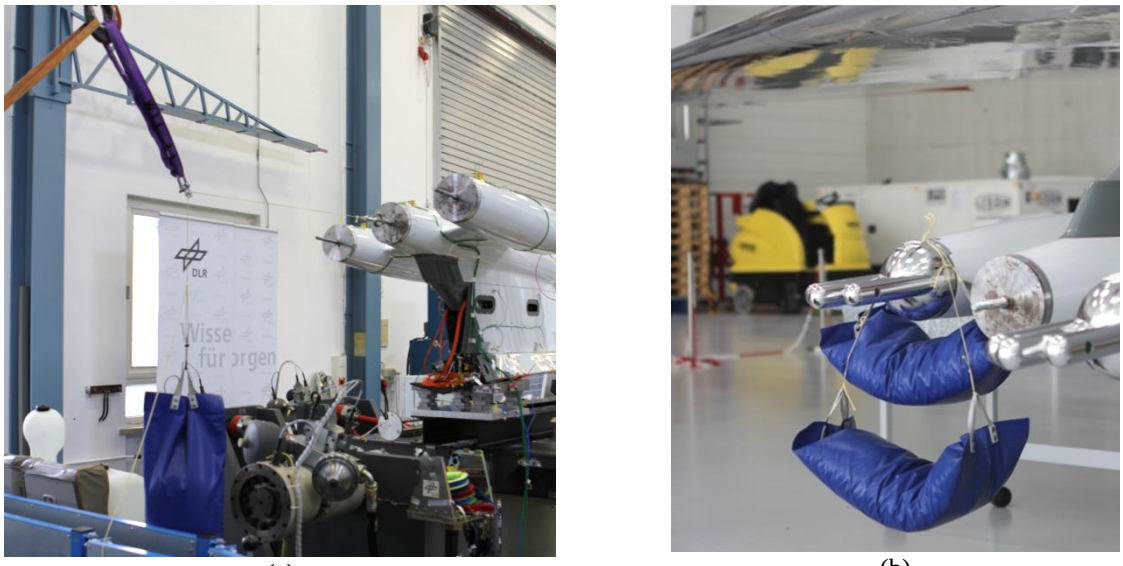

(a) (b)

Figure 11. Load application on PMS carrier during strain gauge calibration in Göttingen (a) and in Oberpfaffenhofen (b)

4.3 Derivation of transfer matrices

In order to obtain the transfer matrix $[\beta]$, Equation (1) is derived to Equation (2), where each row in the matrices $[P]$ and $[\mu]$ stands for each applied load configuration and its corresponding strain signals. For each PMS-carrier the derivation of the matrices were carried out separately.

$$[\beta] = \left[[\mu]^T[\mu]\right]^{-1}[\mu]^T[P] \tag{2}$$

With

$[P]$: applied loads on the PMS-carrier
$[\beta]$: transfer matrix
$[\mu]$: strain signals corresponding to the applied loads

On the one hand, it is possible to include all eight strain gauge bridges to calculate each of the six load components. However this approach would result in large entries in the fully dense matrix $[\beta]$. These large entries would lead to high sensitivity to disturbances or signal noise. Skopinski [8] addressed this as a probable error in the load coefficients.
On the other hand, it is also possible to calculate each load component using only one bridge each. However, this method would lead to a low accuracy of the calculated loads. This aspect is denoted as a probable error in the estimated loads [8].
To avoid this phenomenon, only a few bridges should be considered in the calculation of the loads [9]. For that aim, every combination of the eight bridges is investigated to quantify the accuracy, totaling 255 combinations. As a demonstration, the calculation of probable error in the calculated loads [8] in Equation (3) refers to the lateral force F_y acting on the hanger beam.

$$\gamma_{Fy} = 0.6745 \sqrt{\frac{\sum_1^n {\varepsilon_{Fy}}^2}{n-q}} \tag{3}$$

With

γ_{Fy}: probable error of the lateral forces
n: number of loads applied
q: number of strain gauge bridges taken into account
$\sum_1^n {\varepsilon_{Fy}}^2$: sum of squares of residuals calculated from equation (4)

$$\sum_1^n {\varepsilon_{Fy}}^2 = \sum_1^n {F_y}^2 - \beta_{Fy}[\mu]^T F_y \tag{4}$$

With

F_y: applied lateral forces
β_{Fy}: a column of the matrix $[\beta]$ corresponding to lateral loads F_y, calculated with equation (2) for the corresponding bridge combination
$[\mu]$: strain signals corresponding to the applied loads and bridge combination

To obtain a normalized quantification of the accuracy, the relative probable error $\gamma_{Fy,rel}$ of the lateral force is calculated with Equation (5).

$$\gamma_{Fy,rel} = \frac{\gamma_{Fy}}{\sqrt{\frac{\sum_1^n {F_y}^2}{n-q}}} = 0.6745 \sqrt{\frac{\sum_1^n {\varepsilon_{Fy}}^2}{\sum_1^n {F_y}^2}} \tag{5}$$

With

γ_{Fy}: probable error of the lateral forces
$\gamma_{Fy,rel}$: relative probable error of the lateral forces
F_y: applied lateral forces
n: number of loads applied
q: number of strain gauge bridges taken into account

To quantify the probable error in the load coefficients, Equations (6) and (7) are applied [8].

$$m = \begin{bmatrix} m_{11} \\ \vdots \\ m_{jj} \end{bmatrix} = diag\left(\left[[\mu]^T[\mu]\right]^{-1}\right) \tag{6}$$

With

$[\mu]$: strain signals corresponding to the applied loads and bridge combination

$$\gamma_{\beta Fy,rel} = \gamma_{Fy,rel} \cdot m \tag{7}$$

With

$\gamma_{F\beta y,rel}$: relative probable error of the load coefficients
$\gamma_{Fy,rel}$: relative probable error of the lateral forces

Equations (3) to (7) were applied to all 255 bridge combinations and to all six load components. It turned out that the least relative probable error in the calculated loads $\gamma_{Fy,rel}$ is achieved by using up to eight bridges, whereas the least root mean square of relative probable error in the loads coefficients $rms(\gamma_{F\beta y,rel})$ is achieved by using three or less bridges. To find a compromise between both aspects, the product of both probable errors is calculated for all cases. All three parameters, namely $\gamma_{Fy,rel}$, $rms(\gamma_{F\beta y,rel})$ and their product are taken into account to decide which bridge combination is to be chosen.
After applying the steps for each load component it turned out that the most desirable bridge combination is different for each load component. For this reason, each column of the final transfer matrix $[\beta_{final}]$ – which corresponds to each load component – is filled with entries derived from different bridge combinations. The average number of bridges of both the right and left PMS-carrier taken into account is 3.83. The acquired relative probable errors γ_{rel} with the corresponding numbers of bridges are presented in Table 1.

		F_x	F_y	F_z	M_x	M_y	M_z
Left PMS-carrier	Number of bridges considered	5	5	5	3	3	3
	Relative probable error γ_{rel}	0.395	0.090	0.317	0.111	0.052	0.084
Right PMS-carrier	Number of bridges considered	4	5	6	3	3	3
	Relative probable error γ_{rel}	0.262	0.032	0.160	0.065	0.056	0.081

Table 1. Overview over probable errors of the load components

In Table 1 it is apparent that the estimation of the force components F_x and F_z are in general more inaccurate compared to the rest, because the installed strain gauge bridges have lower sensitivities to the mentioned force components. However, for further analyses the load components which are assumed as more important are among others F_y and M_x.

5 FLIGHT LOADS MEASUREMENT

When conducting the flight test campaign, five flights were performed, the second of which was designated for flight loads measurement. During the flight maneuvers were flown on seven altitudes ranging from 12000 ft to 35000 ft (3658 m to 10668 m) and three airspeeds each. The maneuvers for each flight condition consisted of impulsive inputs on the yoke and rudder pedals, a roll up to ±45° and a pull-up up to 2 g.
Initially, the idea for the flight testing was to achieve flight conditions which evoke significant loads and can be simulated numerically for the validation. An example of such load cases is 1-cos-gusts or atmospheric turbulence. However, the level of natural atmospheric disturbance was not high enough for sufficient natural excitation during the days of the test campaign. Thus, it was discussed to substitute atmospheric gust loads by the definition of manoeuvers with a similar frequency input for that flight. However, to do so stick raps with a frequency of up to 14 Hz would be necessary. Such procedure is difficult to perform with high precision. Besides, the control surface actuation systems would dampen the high frequency input to some degree. Instead, impulsive inputs on the steering system and low frequency maneuvers as described above were considered as safer and easier to perform.
Figure 12 presents the normalized force F_y of both PMS-carriers and the bank angle during a selected roll maneuver. In this case only load increments are considered. This implies that during the steady flight before the maneuver the loads are zero. In Figure 12 it is apparent that

the magnitudes of the forces on both PMS-carriers are not equal; the force experienced during the downward acceleration is larger than during the upward acceleration of the wing.
In Figure 13 the qualitative trend of the vertical force F_z of both PMS-carriers and the angle of attack during a selected pull-up maneuver is shown. It is apparent that the force acting on the PMS-carriers is proportional to the increment of the angle of attack, respectively the vertical acceleration. Since the force F_z in the time interval between 2 s < t < 4 s is negative despite the increase of the angle of attack. It can be concluded that the inertial force acting on the PMS-carrier is larger than the aerodynamic force.

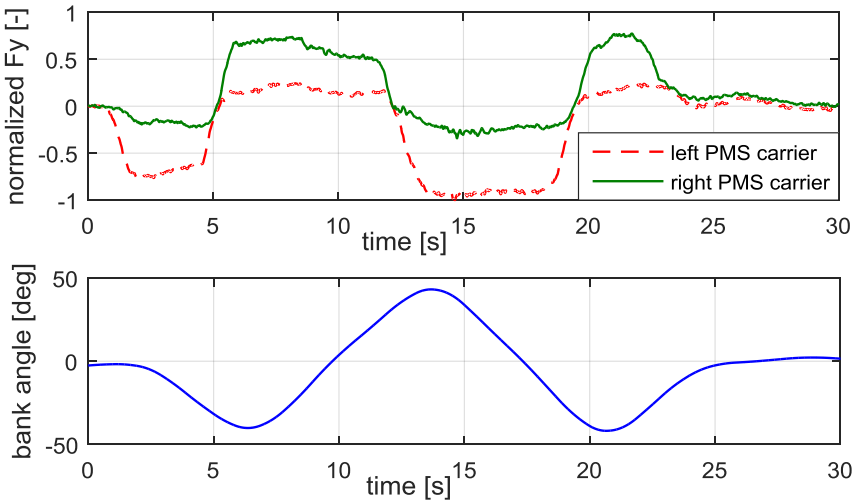

Figure 12. Time history of normalized force *Fy* during a roll maneuver

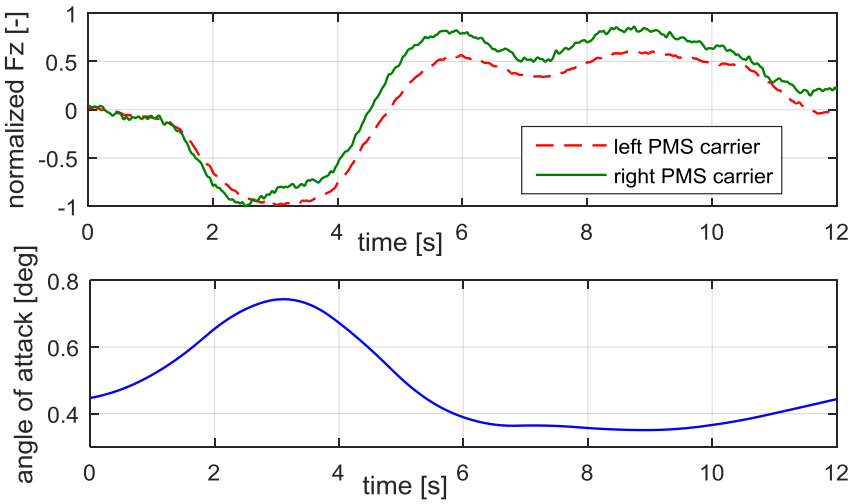

Figure 13. Time history of normalized force *Fz* during a pull-up maneuver

The challenge experienced during the flight testing was among others the temperature drift of the strain signals despite the thermal isolation of the strain gauges, especially during and shortly after altitude changes. This is caused by the concealment of the half of several bridges by aircraft components while the other half was exposed to free stream, since every bridge consists of sensors on opposing sides of the hanger beam. Another challenge was the high stiffness of the hanger beam, therefore the signal to noise ratio is low for certain loading cases. Besides, since the load path through the hanger beam is complex, there is an uncertainty between the optimal strain gauge positions estimated on the available FE model of the shorter hanger beam for the outer station and the actual strain response of the PMS carrier.

6 TURBULENCE MEASUREMENT

During the flight testing the 3D wind field and turbulence data is measured with multi-hole-probes that are installed at the nose boom were also collected. Its first analyses in the frequency domain show that the power spectral density of the measured turbulence in vertical direction is similar to a von-Kármán spectrum, however with a smaller scale turbulence than 2500 ft (762 m) which is defined in CS25[3]. A smaller scale of turbulence implies that the energy of the turbulence is contained in oscillations with higher frequencies. An example of the power spectral density (PSD) of the measured turbulence with a root mean square (RMS) value of 0.14 m/s and reference von-Kármán spectra are depicted in Figure 14, where L stands for the scale of turbulence. The turbulence data was taken at a pressure altitude of 35000 ft (10668 m) during clear weather in the morning and the analyzed time period of 310 seconds. With this type of data, loads analysis methods regarding atmospheric turbulence used by DLR can be compared with the requirements from the regulations.

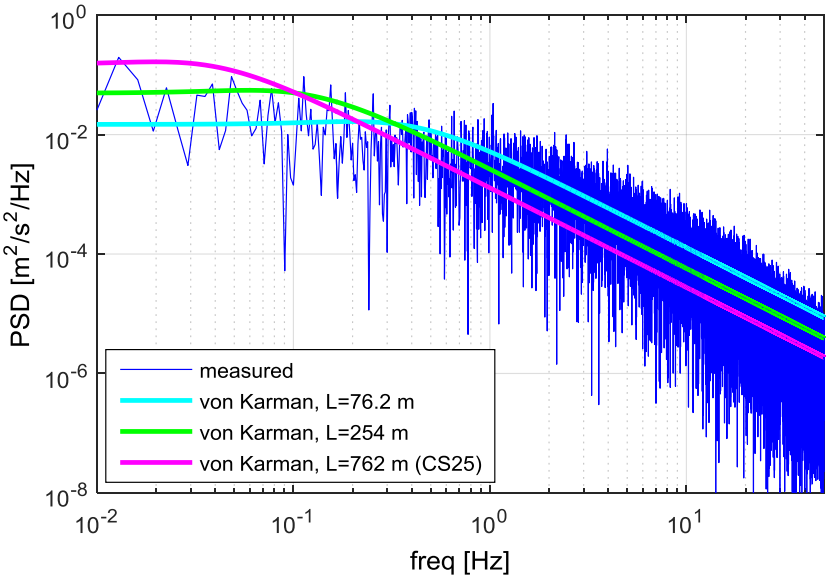

Figure 14. Power spectral density of measured turbulence compared with reference von-Kármán spectra

In the fourth flight the DLR HALO flew together with another aircraft, the DLR Falcon. The aims were to excite elastic modes of DLR HALO by taking advantage of the wake turbulence of DLR Falcon flying ahead of the DLR HALO and to measure the turbulence itself. For the chase flight DLR HALO approached DLR Falcon from behind until the desired level of excitation was reached. The chase flight was performed at two different altitudes and several speeds while taking a sufficient distance between both aircraft into account. An illustration of DLR HALO flying in the wake of DLR Falcon is shown in Figure 15, whereas the latter is at least 1 km in front of DLR HALO.

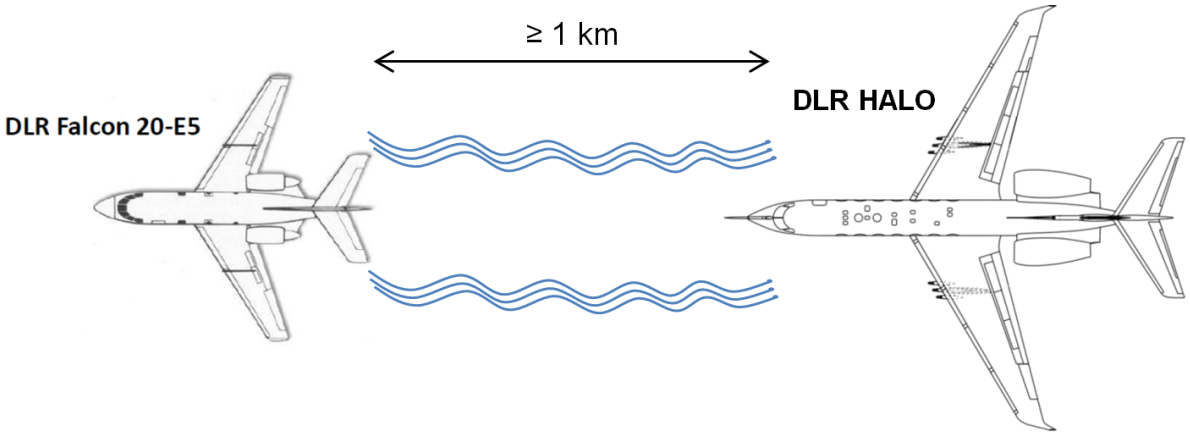

Figure 15. DLR HALO in the wake turbulence of DLR Falcon

An excerpt of the time sequence of the vertical wind speed *wg* is depicted in Figure 16. To distinguish the wake turbulence from the natural turbulence, the graph of the Mach number is also shown. In the wake a higher level of fluctuation of the Mach number is visible. At t = 235 s a transition between the wake and undisturbed flow is visible, where DLR HALO flies out of the wake. During the transition the graph of the vertical wind speed shows a pattern similar to the profile of a free vortex. Such pattern is also visible around t = 210 s, however in this case DLR HALO remains in the wake. At about t = 193 s the graph of the vertical wind speed shows a huge fluctuation with peaks at ±20 m/s. In the graph of the Mach number the fluctuation is also visible, with a maximum increment of approximately 0.1. Furthermore, in the temperature log an increase of 3 K is measured, so it is assumed that the outlier is caused by the engine exhaust of DLR Falcon. Since this disturbance is considered as a local phenomenon registered by the nose boom, the peaks in the vertical wind speed around t = 193 s are neglected in further analyses. Furthermore, it is apparent that in the wake of DLR Falcon the average vertical wind speed is about -4 m/s.

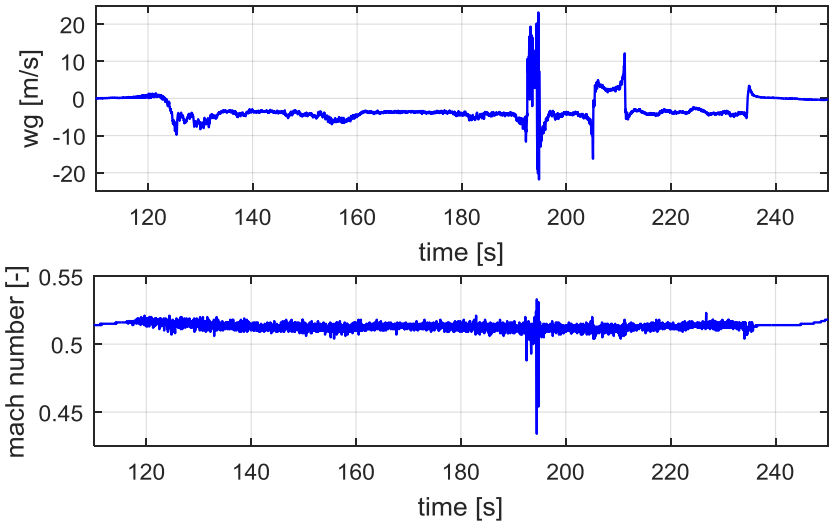

Figure 16. Time history of vertical wind speed and Mach number in the wake

For the turbulence analysis in the frequency domain the considered time sequence begins after the entrance into the wake and ends before the exit out of the wake. The calculated PSD with an RMS value of 2.14 m/s is shown in Figure 17. Not only the RMS is more than 10 times larger than undisturbed flow in Figure 14, but a different distribution is also visible. Contrary to the PSD of undisturbed flow, in this case von-Kármán spectra with longer scale of

turbulence up to 7620 m are more likely to fit the measured wake turbulence. However, this aspect has uncertainty factors, such as the movement of the DLR HALO and therefore its nose boom within the wake. During the flight in the wake the pilot had to correct the aircraft position constantly in order to stay in the wake and to maintain the wings level. Thus it was difficult to keep DLR HALO in a fixed position in the wake, e.g. at the vortex axis for a longer period of time. For this reason the measured turbulence is not representative for determining the flow condition at a certain position of the wake, nevertheless a turbulence spectrum of real aircraft wake could be acquired with this approach.

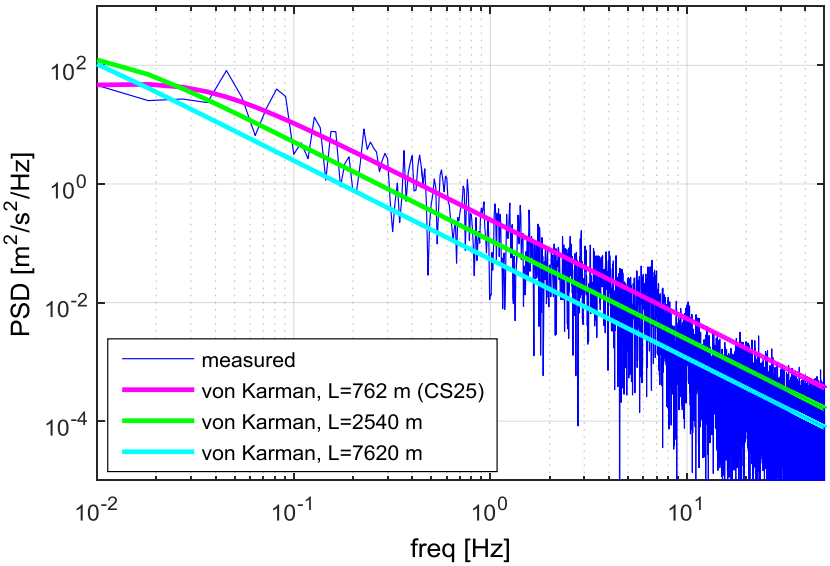

Figure 17. Power spectral density of turbulence in the wake

7 CONCLUSION AND OUTLOOK

The setup of DLR HALO simulation models including the PMS carriers, using the MONA process, and the subsequent loads analysis have been presented. Results from the loads analysis have been extracted to be implemented as an input for a preliminary test of the PMS carrier. The instrumentation of the PMS carriers and their calibration have been illustrated. The DLR HALO test flights relevant for the loads and turbulence measurement have been described. The influence of wake turbulence on the power spectral density of the vertical wind speed has been shown.
The findings acquired through the flight testing deliver a further insight into flight loads and turbulence measurement and its benefit for the DLR loads process [10],[11]. For the evaluation of the flight data, several time histories of the loads have been derived, and for the future further analyses will be conducted to validate the DLR loads process. For a more extensive measurement of flight loads with higher signal to noise ratio a selection of other positions on the aircraft would be necessary, which in turn would lead to longer ground time of the aircraft for the instrumentation and testing. Concerning turbulence measurement, the power spectral densities derived from the measured data can be utilized in the further development of the DLR loads process.

8 ACKNOWLEDGMENTS

The authors thank the colleagues from the department Structural Dynamics and Aeroelastic System Identification as well as the facilities Flight Experiments and Design Organization for the support before, during and after the flight testing.

9 REFERENCES

[1] J. Sinske, Y. Govers, V. Handojo und W. Krüger, "HALO-Flugtest mit instrumentierten Aussenlasten für Aeroelastik- und Lastmessungen im DLR-Projekt iLOADS", *Deutscher Luft- und Raumfahrtkongress*, Braunschweig, Germany, 2016.

[2] J. Schwochow, G. Jelicic, Y. Govers, J. Sinske, R. Buchbach, J. Springer, "Online Monitoring of Aircraft Modal Parameters during Flight Test based on permanent Output-Only Modal Analysis", *AIAA SciTech Forum and Exposition*, Grapevine, Texas, USA, 9.-13.01.2017.

[3] European Aviation Safety Agency, CS25 - Certification Specifications and Acceptable Means of Compliance for Large Aeroplanes - Amendment 16, 2015.

[4] T. Klimmek, "Parameterization of topology and geometry for the multidisciplinary optimization of wing structures", in *CEAS - European Air and Space Conference*, Manchester, United Kingdom, 2009.

[5] W.R. Krüger, T. Klimmek, R. Liepelt, H. Schmidt, S. Waitz, S. Cumnuantip, "Design and aeroelastic assessment of a forward-swept wing aircraft", *CEAS Aeronautical Journal*, Vol. 5, pp. 419–433, 2014.

[6] F van Dalen, A. Rothwell, "Adas structures module: User's manual", Memorandum M-709, TU Delft, 1995.

[7] M.D. Ardema, M.C. Chambers, A.P. Patron, A.S. Hahn, H. Miura, M.D. Moore, "Analytical fuselage and wing weight estimation of transport aircraft", Technical Report Technical Memorandum 110392, NASA, May 1996.

[8] T. Skopinski, W. Aiken Jr. und W. Huston, "Calibration of Strain-Gage Installations in Aircraft Structures for the Measurement of Flight Loads", NACA Technical Note 2993, 1953.

[9] C. Eckstrom, "Flight Loads Measurements Obtained from Calibrated Strain-Gage Bridges Mounted Externally on the Skin of a Low Aspect-Ratio Wing", NASA Technical Note D-8349, 1976.

[10] W.R. Krüger, T. Klimmek, "Definition of a Comprehensive Loads Process in the DLR Project iLOADS", *Deutscher Luft- und Raumfahrtkongress*, 13.-15.09.2016, Braunschweig, Germany, DocumentID: 420105, urn:nbn:de:101:1-201611183243.

[11] T. Klimmek, P. Ohme, P. D. Ciampa, C. Gall, V. Handojo, "Aircraft Loads – An Important Task from Pre-Design to Loads Flight Testing", *Deutscher Luft- und Raumfahrtkongress*, 13.-15.09.2016, Braunschweig, Germany, DocumentID: 420223.

COPYRIGHT STATEMENT